

RESEARCH ARTICLE

Modeling the Role of the Glymphatic Pathway and Cerebral Blood Vessel Properties in Alzheimer's Disease Pathogenesis

Christina Rose Kyrtos^{1,2}, John S. Baras^{2,3*}

1 University of Pittsburgh Medical Center, Department of Neurology, Pittsburgh, Pennsylvania, United States of America, **2** Institute for Systems Research, University of Maryland, College Park, Maryland, United States of America, **3** Department of Electrical and Computer Engineering, University of Maryland, College Park, Maryland, United States of America

* baras@umd.edu



OPEN ACCESS

Citation: Kyrtos CR, Baras JS (2015) Modeling the Role of the Glymphatic Pathway and Cerebral Blood Vessel Properties in Alzheimer's Disease Pathogenesis. PLoS ONE 10(10): e0139574. doi:10.1371/journal.pone.0139574

Editor: Ken Arai, Massachusetts General Hospital/ Harvard Medical School, UNITED STATES

Received: July 3, 2015

Accepted: September 15, 2015

Published: October 8, 2015

Copyright: © 2015 Kyrtos, Baras. This is an open access article distributed under the terms of the [Creative Commons Attribution License](https://creativecommons.org/licenses/by/4.0/), which permits unrestricted use, distribution, and reproduction in any medium, provided the original author and source are credited.

Data Availability Statement: All relevant data are within the paper. Copies of the Matlab files are publicly available at <https://github.com/ckyrtsos/Code-for-PLOS-ONE/blob/master/Code>.

Funding: CRK and JBS were funded by (1) Institute for Systems Research, University of Maryland. www.isr.umd.edu; and (2) University of Maryland Foundation, www.umd.edu (no grant #). The funders had no role in study design, data collection and analysis, decision to publish, or preparation of the manuscript.

Abstract

Alzheimer's disease (AD) is the most common cause of dementia in the elderly, affecting over 10% population over the age of 65 years. Clinically, AD is described by the symptom set of short term memory loss and cognitive decline, changes in mentation and behavior, and eventually long-term memory deficit as the disease progresses. On imaging studies, significant atrophy with subsequent increase in ventricular volume have been observed. Pathology on post-mortem brain specimens demonstrates the classic findings of increased beta amyloid (A β) deposition and the presence of neurofibrillary tangles (NFTs) within affected neurons. Neuroinflammation, dysregulation of blood-brain barrier transport and clearance, deposition of A β in cerebral blood vessels, vascular risk factors such as atherosclerosis and diabetes, and the presence of the apolipoprotein E4 allele have all been identified as playing possible roles in AD pathogenesis. Recent research has demonstrated the importance of the glymphatic system in the clearance of A β from the brain via the perivascular space surrounding cerebral blood vessels. Given the variety of hypotheses that have been proposed for AD pathogenesis, an interconnected, multilayer model offers a unique opportunity to combine these ideas into a single unifying model. Results of this model demonstrate the importance of vessel stiffness and heart rate in maintaining adequate clearance of A β from the brain.

Introduction

Alzheimer's disease (AD) is a multi-faceted, progressive neurodegenerative disease. It is the most common cause of dementia in the elderly, affecting nearly 1 in 8 individuals over the age of 65 in the United States [1]. AD has been clinically described by the symptoms of short-term memory deficits, cognitive decline and eventual long-term memory deficit. These deficits lead

Competing Interests: The authors have declared that no competing interests exist.

to a decreased quality of life, often eventually requiring assistance with activities of daily living (ADLs) in a long term care setting [1–2]. There is a tremendous burden for the cost of care even though no preventative or curative treatments are available. Given the increasing number of the elderly affected by AD and the lack of any viable treatment options, there is a pressing need to develop a better understanding of the disease process as well as effective treatment modalities.

Beta amyloid levels within the brain, particularly the oligomeric form, are linked to the loss of neurons, stimulation of neuroinflammation, abnormal mitochondrial function and increase in tau levels [3–10]. Decreased clearance of A β from the brain via the glymphatic system and the low-density lipoprotein-related receptor 1 (LRP-1) have been implicated in the pathogenesis of AD, and have been known to occur in normal aging as well [11–12]. The glymphatic system (located in the perivascular space) is believed to drain approximately 60% of the brain A β to cervical lymph nodes using convective flow generated by arterial pulsations [13–16]. Increased vessel stiffness causing decreased flow of brain interstitial fluid (ISF) is believed to lead to decreased A β clearance with aging [14, 17]. As A β concentration builds within the perivascular space, deposition occurs slowly, eventually leading to the breakdown of the blood-brain barrier secondary to degeneration of smooth muscle cells and brain endothelial cells [14]. Beta amyloid deposition in blood vessels has also been shown to inhibit angiogenesis, impair vascular tone and decrease local cerebral perfusion [14, 18]. Clearance of A β by LRP-1 has also been shown to decrease by nearly 55% during aging and is believed to be secondary to loss of brain endothelial cells [19].

Given the complex nature of cellular and molecular interactions, mathematical modeling offers a unique opportunity to further understand the pathogenesis of AD. Several other mathematical models of AD have been proposed, with the majority focusing on A β fibril nucleation and growth of A β plaques [20–21]. Puri and Li developed a network model to study the interactions between neurons, astrocytes and microglia, while Luca et al presented a model on microglia chemotaxis towards A β [22–23]. However, there has been no model developed to study the transport of A β from generation at the neuron to clearance at the blood-brain barrier or via the glymphatic (eg. perivascular) pathway.

The model presented in this paper studies how A β levels change within the brain parenchyma and vasculature during normal aging while incorporating the role of the glymphatic system. Conservation of mass equations are used to model A β levels. Neurons, microglia and brain endothelial cells interacted dynamically and responded to both parameters determined by aging process, as well as with the A β levels. The role of increased vessel stiffness secondary to aging, prolonged hypertension and cerebrovasculature deposition of A β , as well as alterations in heart rate, were also studied given the correlation between cardiovascular risk factors and AD. The results of this model demonstrate the importance of maintaining healthy cardiovascular function and offer insight into possible preventive or treatment options in the future.

Methods

Model Assumptions

This model describes the flow of several key chemical species within a 1 mm³ volume of CA1 hippocampal tissue (volume of CA1 in healthy patients is approximately 640 mm³, total hippocampal volume in healthy patients is around 2100 mm³) [24]. The system is divided into three compartments: the blood within the nearby cerebral capillaries; the blood-brain barrier (BBB) and associated perivascular space; and the brain parenchyma, respectively. Capillaries are aligned in parallel with a separation distance of 40 μ m [25] and assumed to have a linear segment length of 1 mm. Neurons and microglia reside within the brain parenchyma between the

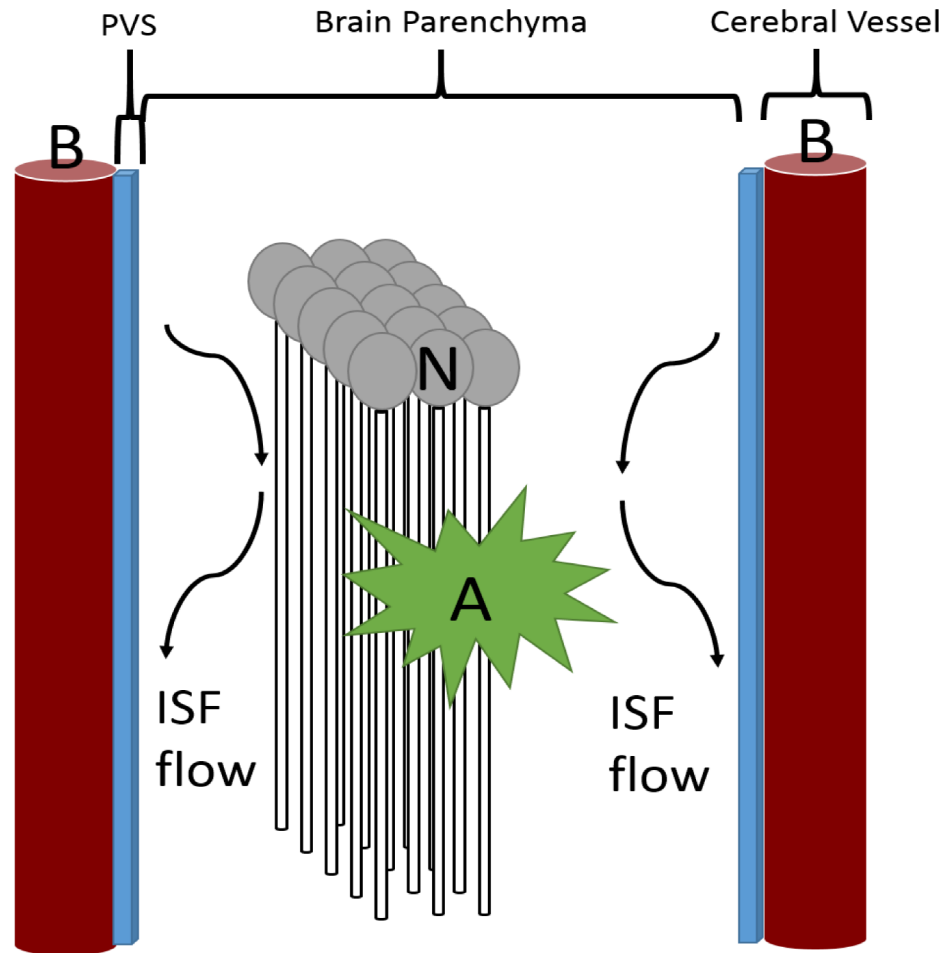


Fig 1. Three compartment model used for modeling. The brain was divided into the brain parenchyma, containing the neurons (N) and astrocytes (A); the perivascular space (PVS, blue strip) in the area between the astrocytic foot processes and the brain endothelial cells; and the cerebral blood vessels (B). Interstitial (ISF) flow is unidirectional and laminar in the regions lined by capillaries; its rate is dependent on heart rate (eg. the rate of arterial pulsations) as well as the stiffness of the vessels, which is a function of the presence of atherosclerosis, cerebral amyloid angiopathy (deposition of beta amyloid within the brain vessels) and stiffening secondary to prolonged elevations in systemic blood pressure.

doi:10.1371/journal.pone.0139574.g001

capillaries and are assumed to have a uniform density. [Fig 1](#) demonstrates the overall layout of the system being modeled.

Each compartment is assumed to be well-mixed with uniform spatial distribution. From recent studies, it has been demonstrated that $A\beta$ is quickly transported from the site of generation via a combination of diffusion (diffusion coefficient, D , range of $1.6\text{--}6.23 \times 10^{-7} \text{ cm}^2/\text{s}$ for monomers to $4 \times 10^{-9} \text{ cm}^2/\text{s}$ for oligomers) and convective flow via the bulk brain ISF ($0.1\text{--}0.3 \mu\text{m}/\text{min}/\text{g}$ brain tissue [26–28]). Spatial variation of chemical species such as $A\beta$ does occur, however, the time course of this variation given the relatively small intercapillary distance ($40 \mu\text{m}$ [25]) is negligible compared to the time scale used in the simulation.

Beta amyloid is generated by neurons within the brain parenchyma, rapidly mix with brain ISF, and $A\beta$ is transported towards the blood-brain barrier for further transport or clearance [15, 29]. Brain ISF flows along the basement membrane of capillaries and arterioles, to the walls of cortical and leptomeningeal arteries, to the base of the skull before exiting the brain for

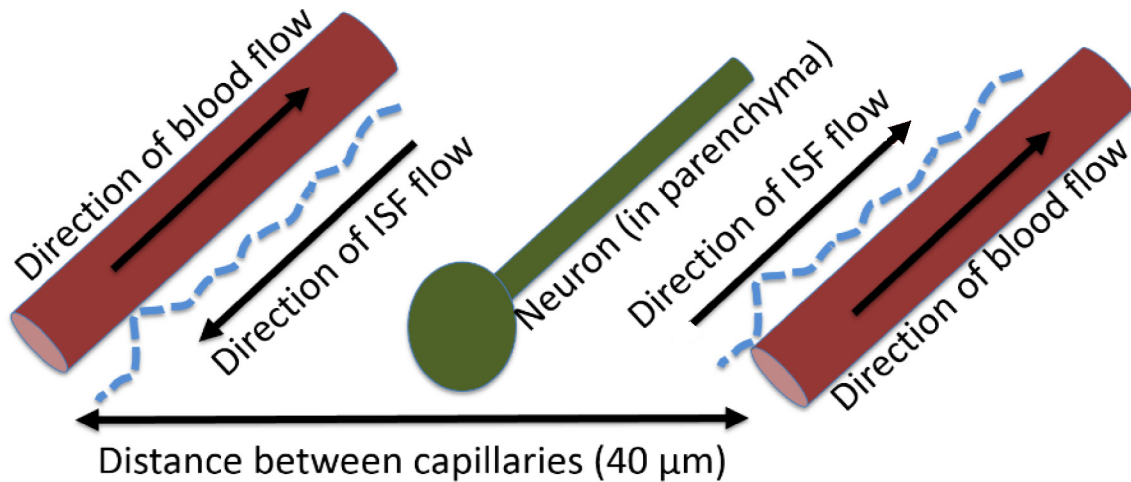


Fig 2. Flow of brain interstitial fluid in response to pulsations of cerebral arteries and arterioles. Interstitial fluid is generated at the brain endothelium by an unclear process [30] and surrounds neurons, microglia astrocytes and other cells located within the brain parenchyma, bringing nutrition to the cells and removing wastes. Although its chemical composition is similar to cerebrospinal fluid (CSF), the two fluids serve separate purposes. CSF gives the brain buoyancy and buffers against forces applied to the head; CSF is generated by ependymal cells within the choroid plexus [30]. Brain ISF transports waste from the brain parenchyma via a combination of convection and diffusion towards the perivascular space. At the perivascular space, molecules such as $A\beta$, are either transported by receptors at the blood-brain barrier, or are transported along the glymphatic pathway. A small percentage of molecules transported in the perivascular space are transported into the cerebrospinal fluid at the arachnoid granulations and are cleared from the brain via CSF drainage pathways. The majority (~60%) of $A\beta$ is transported along the glymphatic system to the cervical lymph nodes [13].

doi:10.1371/journal.pone.0139574.g002

the cervical lymph nodes [14]. It is not known whether significant levels of transported substances build-up at the cervical lymph nodes. ISF flow is assumed to be unidirectional, well-mixed, and originating from the pulsations of arterial vessels in response to the cardiac cycle (Fig 2). There is some debate in the literature as to whether glymphatic flow is in the same or opposite direction as cerebral blood flow; this model assumes that flow is in the same direction [13, 16]. ISF flow rate is dependent on the heart rate, the ability of the vessel wall to transmit pulsations (eg. the compliance of the arterial wall). Arterial wall compliance can be estimated by wall stiffness (S), which increases with age, hyalinosis secondary to prolonged hypertension, atherosclerosis and vasculitis [14–15]. It is important to note that although brain ISF is generated by brain endothelial cells at the capillary and other vessels, only the arteries and arterioles possess the smooth muscle cells necessary to produce the pulsations to cause ISF flow [30–31].

Once transported to the blood, molecules are rapidly cleared away at a rate of once per second (assuming a heart rate of 60 beats per minute). The blood has also been assumed to be well-mixed and serves as a relative sink for $A\beta$. Although viscosity of blood can change during aging and disease (eg. diabetes, dehydration), we have not modeled these changes here and assumed that the viscosity and physical properties of blood remain constant throughout the simulation.

Model Derivation

Cell numbers. The volume of the hippocampus has been estimated by both neuropathology and magnetic resonance imaging (MRI) in healthy controls, as well as in patients with mild cognitive impairment (MCI) and AD [24, 32]. Follow-up MRI imaging demonstrated a significant increase in the rate of volume loss in patients with AD or MCI of nearly 5 and 3 times, respectively, the rate of volume loss in healthy controls (table 1) [24]. The total neurons loss in the CA1 region during an average course of AD (15–20 years) has been estimated at 50–60%, much faster than that observed with normal loss during aging (1%, or a 50% loss over 69 years), and demonstrating the impact that the faster loss rate has on the AD-afflicted brain.

Table 1. Volume of the human hippocampus as determined by MRI.

Patient	Healthy	MCI	AD
Baseline volume (mm ³)	2133 (25)	1846 (23)	1631 (34)
Rate of loss/year (mm ³ /yr)	-17.3 (10.5)	-47.5 (6.5)	-72.0 (9)
% loss/year (%/yr)	-0.8 (0.5)	-2.6 (0.3)	-4.4 (0.6)

MCI, mild cognitive impairment; AD, Alzheimer's disease. Volume loss was approximately 1% in healthy controls, 2.5% in MCI and 4.5% in AD patients. The rate of loss in AD patients was noted to increase by 1.4%/year (total rate of 5.8%.year) in patients with AD carrying the ApoE4 allele. Values are given as the mean with standard deviation in parentheses.

doi:10.1371/journal.pone.0139574.t001

The number of neurons located in the CA1 region of the hippocampus was estimated from the works of Harding and Zarow [33–34]. Zarow et al described the changes in neuron number with respect to the Braak staging, and found that patients with a Braak stage of 0 (essentially healthy, no presence of neurofibrillary tangles) had approximately 3.25×10^6 CA1 neurons, while those with a Braak score of 6 (severe AD pathology) had only 1.5×10^6 CA1 neurons [34]. The maximum number of CA1 neurons reported [33] was 6.14×10^6 . Total volume of the CA1 was estimated to be $641 \pm 153 \text{ mm}^3$ in healthy normal patients, decreasing to $377.5 \pm 132 \text{ mm}^3$ in patients with AD [32]. From this, we derived the density of neurons in the CA1 region to be $5275/\text{mm}^3$ ($4050\text{--}6500/\text{mm}^3$) in healthy controls and $4500/\text{mm}^3$ (range 3000–6000) in AD [17, 35–37]. The change in neuron number over time can thus be described by:

$$\frac{dN}{dt} = (1 - (k_1 + d))N(t) \tag{1}$$

where d is the natural rate of neuron loss in the healthy control, k_1 is the additional neuron loss due to increased beta amyloid levels seen in AD or the presence of the ApoE4 allele, and N is the number of neurons within the control volume.

The density of microglia within several brain regions has been estimated via neuropathology. Tetreault et al found that the average density microglial density in the neocortex is approximately $5951 \text{ microglia}/\text{mm}^3$ [38]. The total number of microglia has been found to vary depending on gender, with women only having 1.9×10^9 and men having 2×10^9 microglia [39]. Calculating the microglial density from these values, also noting the slightly lower average brain volume for women, we find that microglial density in women is about $3080 \text{ microglia}/\text{mm}^3$ and $3420 \text{ microglia}/\text{mm}^3$ in men [39]. The number of microglia were also found to decrease over time secondary to dystrophy at a conversion rate of about 80% by 65 years old [40]. Given this range, the microglia density was set at $4500 \text{ microglia}/\text{mm}^3$ with a conversion to dystrophy rate of $7.3 \times 10^{-5}/\text{day}$. The equation for microglia number is given by:

$$\frac{dM}{dt} = (1 - k_{12})M(t) \tag{2}$$

where k_{12} is the conversion to dystrophy rate and M is the number of microglia within the modeled volume.

Brain endothelial cells (ECs) line cerebral capillaries and work with astrocytes to form the blood-brain barrier (BBB). Between the astrocyte foot processes and the endothelial cells is the perivascular space (PVS), a narrow space (50–100 nm) composed of the basement membrane that allows movement of brain ISF from the capillaries towards the arteries [12, 14, 41]. Endothelial cells in low-flow vessels (such as capillaries) have been found to take on a hexagonal or polygonal shape, with only a single endothelial cell wrapping end-to-end to form the capillary

wall. Given that the average capillary wall is approximately 8 μm in diameter, the circumference of the “wrapped” brain capillary endothelial cells can be estimated as 25 μm . Polygonal endothelial cells with this length have been estimated to be between 10–20 μm in width [42–44]. For modeling purposes, we have assumed the final dimensions to be 25 by 20 μm , or approximately 5 endothelial cells per 100 μm capillary length.

Brain ECs have a natural replacement rate of 0.1% per day [45–46], increasing to 1–10% per day if ECs are being exposed to high blood pressure or turbulent flow [45]. During mitosis and EC replacement, some cells are abnormally created leading to EC senescence. This is a process where endothelial cells divide to replace damaged cells and maintain the capillary wall, however, there is local breakdown of the BBB as tight junctions fail to form correctly [47–48]. Denuded spots and disruption of capillary laminar flow have been hypothesized to occur with senescence [47–48]. Approximately 3–7% of ECs are senescent in a 65 year old exposed to normal stressors; this rate increases to 41–93% senescence when ECs are exposed to only twice the level of stressors [47]. Assuming the higher rates of senescence, this translates to a senescence rate of 0.1% per year under normal conditions and 1.4% per year under increased stressors. The equation for the number of brain ECs is then given by:

$$\frac{dEC}{dt} = (1 - k_2)EC(t) \tag{3}$$

where k_2 is the rate of ECs entering senescence and EC is the number of brain endothelial cells lining the capillaries in the model volume.

Chemical Species

Beta amyloid. Beta amyloid is generated by neurons after the sequential processing of the amyloid precursor protein (APP) by β - and γ -secretase and is found deposited in both the brain parenchyma as well as the cerebral vasculature. The generation rate has been estimated as 3×10^{-4} pg per neuron per day, or the equivalent order of 10^4 molecules per neuron per day [2]. The ratio of $A\beta_{42}$ to $A\beta_{40}$ generation has been found to be approximately 1:5 [49]. From this data, the generation rate for $A\beta_{40}$ was set at 1.6×10^4 and $A\beta_{42}$ was set at 3×10^3 . The average concentration of $A\beta$ within brain parenchyma has been estimated using both mice and human brains. Marklund et al used microdialysis probes placed into the brains of patients following traumatic brain injury and noted average $A\beta_{40}$ levels of 436 pg/mL (range 281.3–971.3 pg/mL) and $A\beta_{42}$ levels of 60 pg/mL (range 46–90 pg/mL; values measured in patients with focal brain injury away from the site of injury) [5]. Studies using human brain homogenates have shown similar results (73 pg/mL for $A\beta_{42}$ and 440 pg/mL for $A\beta_{40}$) [35]. Using this range, the initial concentrations for $A\beta_{40}$ and $A\beta_{42}$ are 450 pg/mL and 70 pg/mL, respectively. The general conservation of mass equation can be used to define the change of $A\beta$ within the brain parenchyma as:

$$\frac{\partial C}{\partial t} = -\nabla N + R, \text{ where } N = D\nabla C + vC \tag{4}$$

where N is the molar flux, D is the diffusion coefficient of $A\beta$, C is the volume concentration of $A\beta$, v is the fully developed velocity of the ISF, and R is the volumetric rate of chemical reactions taking place within the control volume given by the rate of $A\beta$ transport by LRP-1 at the BBB. Given the assumptions that flow is unidirectional, fully developed and laminar (given the small length scales modeled) in the region modeled, this equation can be further simplified as:

$$\frac{dC}{dt} = -v \frac{dC}{dx} - R \tag{5}$$

where R represents the generation of $A\beta$ (k_3, k_4), the rate of uptake by microglia (k_5), and the rate of deposition within the brain parenchyma (k_{7a}). Degradation of $A\beta$ by extracellular enzymes such as neprilysin have been shown to be negligible *in vivo* [19, 50]. The final equation for $A\beta$ within the brain parenchyma is given by:

$$\frac{dC_1}{dt} = -v \frac{dC}{dx} + k_3 k_4 N(t) - k_5 M(t) - k_{7a} C_1(t) \tag{6}$$

The concentration of $A\beta$ in the perivascular space (C_2 for $A\beta_{40}$ and C_5 for $A\beta_{42}$) is derived using a similar simplification of Eq (5) where the concentration differential is still between the brain ISF and the perivascular space. The velocity of the bulk ISF flow was assumed to be approximately double that in an older person and was accounted for in the model. The reaction term is described by the transport rate of $A\beta$ by LRP-1 at the BBB (k_6) and the rate of deposition in the perivascular space (k_7):

$$\frac{dC_2}{dt} = v \frac{dC}{dx} - k_6 \left(\frac{LRP(t)}{LRP_0} \right) C_2(t) - k_7 C_2(t) \tag{7}$$

where LRP_0 is the initial concentration of LRP-1 receptors on the brain endothelial cells. A similar equation is used to calculate the $A\beta_{42}$ concentration in the perivascular space (C_4) with rate constant k_7 replaced with k_{9a} . A term for ApoE was not directly included in Eq (7) given the recent evidence that ApoE may not play a significant role in $A\beta$ clearance by LRP-1 and may actually, in fact, be a competitive inhibitor of $A\beta$ transport since both bind to the LRP-1 receptor [15, 51–52]. Further evidence for this possibility was shown by Shibata et al who noted that there was minimal difference in transport rates in wild-type mice versus ApoE knockout mice [19]. Bell et al confirmed this in their studies of $A\beta$ clearance by LRP-1 and demonstrated that the clearance rate of $A\beta$ bound to ApoE was only about 10% the transport rate of $A\beta$ alone [53]. There is an effect of the ApoE allele, however, on the amount of $A\beta$ transported by LRP-1, as it is believed that ApoE4 may actually bind to LRP-1 longer, thus, increasing potential inhibition of the LRP-1 receptor and slowing clearance of $A\beta$ from the brain [52]. Bachmeier et al demonstrated that clearance of LRP-1 decreased by approximately 2.5 times when the ApoE4 allele was compared to the ApoE3 allele [54].

Review of the literature demonstrated a wide range of transport rates for LRP-1, ranging from 0.015/min to 0.03/min of the fraction of $A\beta_{40}$ injected [19, 55–56]. Bell et al measured the transport rate constant in pmol/min/gram of ISF and found the rate to be 0.211 for $A\beta_{40}$ and 0.111 for $A\beta_{42}$ [53]. Using the conversion for density of brain tissue of 0.99g/cm³ [57], this would be equivalent to 12x10⁷ molecules/min/mm³ brain, which is more than a magnitude of order elevated beyond the steady state concentration that has been measured *in vivo*. Given the disparity and incongruency in the LRP-1 rate constants in the literature, we used the assumption that 40% of $A\beta$ is cleared by LRP, while the remaining $A\beta$ is cleared by the perivascular pathway or is deposited [11]. This rate of clearance decreased with aging as the density of LRP-1 receptors decreased in response to declining numbers of functioning brain endothelial cells.

Deposition of $A\beta$ within the brain parenchyma (C_9) occurred at a constant rate over time dependent on the concentration of $A\beta$:

$$\frac{dC_9}{dt} = k_{7a} C_1(t) \text{ for } A\beta_{40}; \quad \frac{dC_{10}}{dt} = k_9 C_4(t) \text{ for } A\beta_{42} \tag{8}$$

where C_1 is the concentration of $A\beta_{40}$ within the brain parenchyma and C_4 is the concentration of $A\beta_{42}$ in brain ISF. Deposition of $A\beta$ within the cerebral vessel similarly occurred at a

constant rate related to the Aβ concentration within the perivascular space:

$$\frac{dC_3}{dt} = k_7 C_2(t) \text{ for } A\beta_{40}; \quad \frac{dC_6}{dt} = k_9 C_5(t) \text{ for } A\beta_{42} \quad (9)$$

LRP density. The density of the LRP-1 receptor on brain endothelial cells was determined experimentally by Hvidberg et al to be approximately 31 fmol/mm³ [58]. In the model, a 1mm² area would contain an array of 21 by 21 capillaries. The depth of this array would contain 50 brain ECs, thus, the total density of LRP-1 receptors in the model volume (1mm³) would be 9.3x10¹¹. During normal aging, the total number of LRP-1 receptors in a given volume decreases by about 55% [19]. Assuming that this loss occurs secondary to the loss of brain endothelial cells with, the rate of LRP-1 loss (k₁₀) is equal to the rate of loss of endothelial cells (k₂):

$$\frac{dLRP}{dt} = (1 - k_{10})LRP(t) \quad (10)$$

The values for each of the rate constants are given in Table 2.

Simulation conditions. The model was simulated using Matlab. Initial conditions assumed that the model described a 30 year old and was run for a total of 50 years. The time-step used was a single day. Thus, a total of 18,250 data points were determined. Sensitivity analysis was completed for rate constants that were estimated (initial concentration in perivascular space, increased generation of Aβ when a stimulus is present).

Table 2. Rate constants and initial conditions used in modeling.

Variable	Represents	Units	Value	Reference
N	# of neurons	#/volume	5275 (4050–6500)	5, 7–8, 11, 20
M	# of microglia	#/volume	4500 (3000–6000)	23–24
EC	# of brain ECs	#/length	5 per 100μm (capillaries)	9, 12, 18, 26
C₁/C₄	Initial Aβ conc. in brain ISF	pg/ml	Aβ ₄₀ : 450 (240–770) Aβ ₄₂ : 70 (40–100)	5, 8, 17
C₂/C₅	Initial Aβ conc. in PVS	mass/vol	10% C ₁ /C ₄	Model assumption
C₃/C₆	Concentration of Aβ in vessels	mass/vol	0 (initially)	Model assumption
C₉/C₁₀	Conc. of Aβ deposited in brain	mass/vol	0 (initially)	Model assumption
k₁	Loss of neurons when stimulated	%/time	3.4%/yr	7–8
d	Natural rate of neuron loss	%/time	1%/yr	7–8
k₂	Loss of ECs	%/time	0.1%/yr (no stim) 1.7%/yr (stim)	16, 19
k₃/k₈	Aβ _{40/42} generation rate	#/neuron/ time	Aβ ₄₀ : 16000 Aβ ₄₂ : 3000	15
k₄	Stimulated Aβ generation rate	%/time	1.5	Estimate
k₅/k₁₁	Microglia uptake rate	#/microglia/ time	Aβ ₄₀ : 1400 Aβ ₄₂ : 200	Estimated from 3–4
k₆	Aβ transport rate constant for LRP	1/time	ApoE2/3: 0.4 ApoE4: 0.12	2, 21
k₇/k_{9a}	Aβ deposition rate in vessels	fraction/day	Aβ ₄₀ : 0.004 Aβ ₄₂ : 0.002	6, 21
k₉/k_{7a}	Aβ deposition rate in brain	fraction/day	Aβ ₄₀ : 0.001 Aβ ₄₂ : 0.001	6, 21

Values were derived from experimental studies or estimated given available data. We assumed that there was no Aβ deposited in the brain parenchyma or cerebral vessels at the beginning of the simulation.

doi:10.1371/journal.pone.0139574.t002

Results

The objective for the model was to study the role that aging has on the clearance of $A\beta$ via the perivascular pathway and transport at the blood-brain barrier by LRP-1. Normal aging causes a slow, steady decrease in the number of neurons in the brain with minor accumulation of $A\beta$ within brain parenchyma and cerebral vessels in the majority of individuals. This was demonstrated clearly in our simulation of normal aging (Fig 3).

Heart rate leading to arterial pulsations is important for maintaining the clearance provided by the perivascular glymphatic pathway. During aging, it is common for patients to develop heart rate abnormalities, either too slow of a heart rate (bradycardia), too fast (tachycardia) or an abnormal rate (atrial fibrillation). We hypothesized prior to running simulations that having bradycardia would lead to a decreased $A\beta$ clearance rate and thus, lead to an elevation in $A\beta$ deposition. Conversely, we postulated that an elevated heart rate (for example, from exercising daily) would help to increase the clearance rate and thus decrease the amount of $A\beta$ available for deposition. This was in fact what was seen (Fig 4), with the amount of $A\beta$ deposition in the brain parenchyma increasing by about 20% while deposition within cerebral vessels was minimal (about 5%). Additionally, an elevated heart provided slightly better survival for neuron number.

The stiffness of blood vessels is known to increase over time with aging. Vessel stiffness can also increase significantly in diseases such as atherosclerosis and cerebral amyloid angiopathy, two diseases that increase the risk of transitioning to AD in older age. Increasing the stiffness of vessels by a factor of 2 over the course of the simulation via an exponential rise, surprisingly, led to a significant increase in $A\beta$ deposition within brain parenchyma with $A\beta_{40}$ increasing nearly 100x and $A\beta_{42}$ increasing greater than a factor of 10^3 , a level often seen in the brains of those with AD (Fig 5). Beta amyloid deposited within cerebral vessels actually decreased, most likely secondary to less $A\beta$ reaching the perivascular space by convection alone. There was also increased neuronal cell death given the high $A\beta$ levels, with neuron number decreasing to about $\frac{1}{2}$ of the normal age-matched simulation.

The ApoE4 allele is a well-known risk factor for having late-onset AD and is found in 65–80% of all AD cases [59]. Approximately 15–20% of the population is a carrier for ApoE4 (either homozygote or heterozygote), and thus, have an increased risk of AD. The other two alleles (ApoE2 and ApoE3) are not known to contribute to AD risk and are carried by 5–10% and 65–70% of the population, respectively [59]. It is believed that the ApoE4 allele may contribute to elevated $A\beta$ levels by either competitively inhibiting $A\beta$ binding to LRP-1, or by causing inefficient binding of the ApoE* $A\beta$ complex to LRP-1 [51, 59]. Decreasing the transport rate of $A\beta$ by LRP-1 by 2.5 times over the course of the simulation led to approximately a two-fold increase in $A\beta_{40}$ deposition and a 67% increase in $A\beta_{42}$ deposition in cerebral vessels. There was no additional accumulation of $A\beta$ within the brain parenchyma or changes in cell number (Fig 6).

The final simulations studied the effect of multiple risk factors on changes in $A\beta$ levels. Of the risk factors studied, heart rate and vessel stiffness were the two that could be somewhat modifiable. In Fig 7a, we show that the combination of the ApoE4 allele with bradycardia led to an increase in all $A\beta$ parameters measured, with the most significant increase in $A\beta_{40}$ in cerebral vessels. There was a minimal decrease of less than 10% in the number of neurons. In Fig 7b, we studied the effect of having both the ApoE4 allele as well as a two-fold increase in vessel stiffness. This combination led to a significant increase in $A\beta$ deposition within the brain parenchyma of both forms ($A\beta_{42} > A\beta_{40}$). Beta amyloid deposition within the cerebral vessels was decreased compared to normal aging, however, this decrease was not as severe as that seen in with only increased stiffness. This suggests that ApoE has more of an effect on the deposition of $A\beta$ within the cerebral vessels rather than the brain parenchyma. There was significant

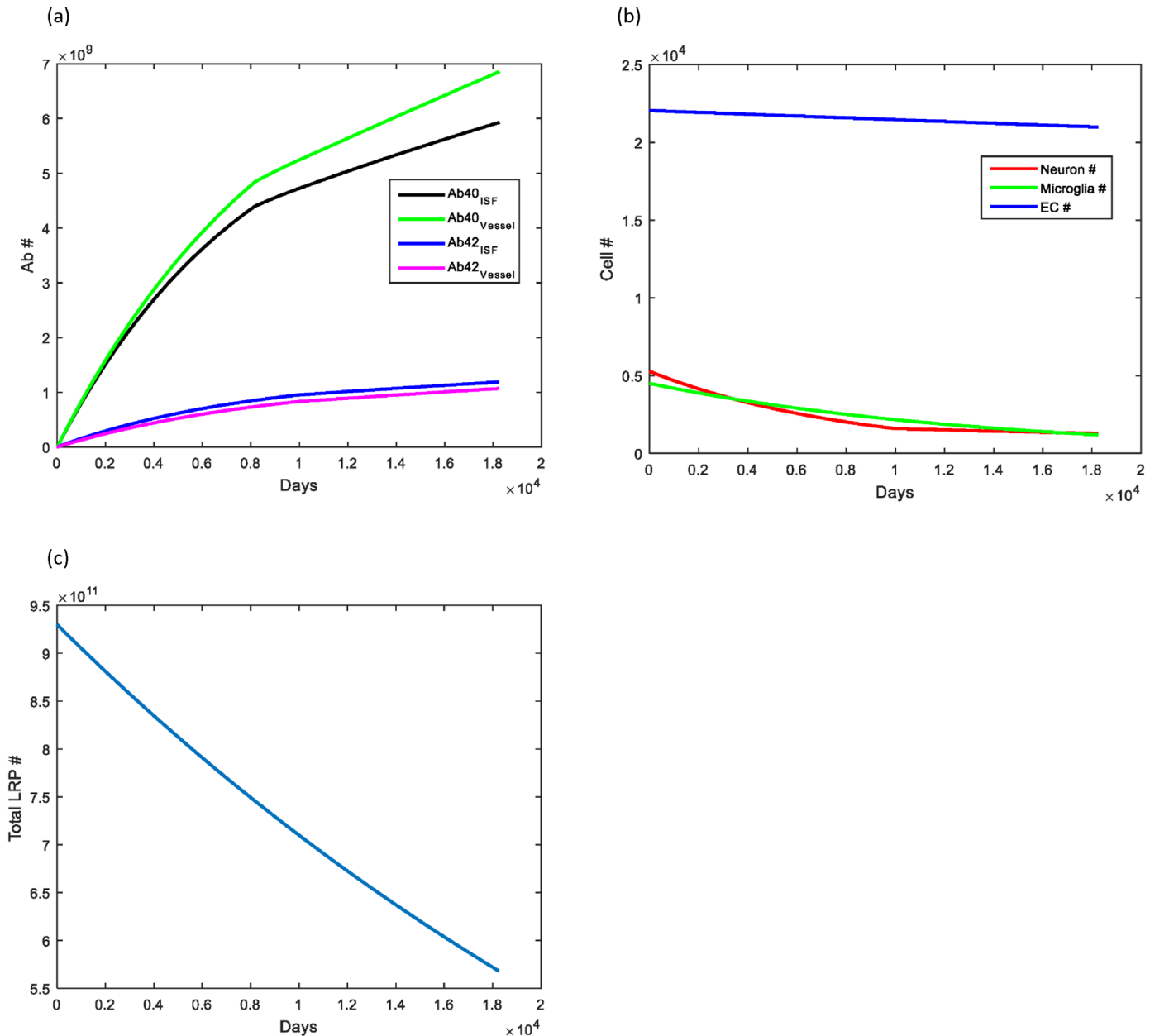


Fig 3. Simulation demonstrating effects of normal aging on Aβ levels within the brain parenchyma and local cerebral vessels. (A) Deposition of Aβ40 occurred much more rapidly than that of Aβ42 with approximately 6 times the amount of Aβ40 deposited within cerebral vessels. This ratio agrees with what has been observed experimentally. The rate of Aβ increase started to decrease over the simulation as the number of neurons declined with aging and from elevations in the Aβ concentration. (B) The number of endothelial cells (blue) decreased slowly as they entered senescence. Microglia (green) decreased about 80% from their initial values, correlating with conversion to dystrophy. Neurons (red) also decreased secondary to natural loss as well as loss from elevated Aβ levels. (C) The total number of LRP-1 receptors decreased to approximately 60% of the initial value in accordance with the loss of brain endothelial cells.

doi:10.1371/journal.pone.0139574.g003

neuronal loss in this simulation, with no changes noted in the microglia or endothelial cell number. Fig 7c shows the effect of increased vessel stiffness with bradycardia. The results of this simulation were nearly identical to those of increased stiffness alone, suggesting that the effect of bradycardia when there is underlying cardiovascular dysfunction (increased vessel stiffness) is minimal. A summary of the results for each simulation are included in Table 3.

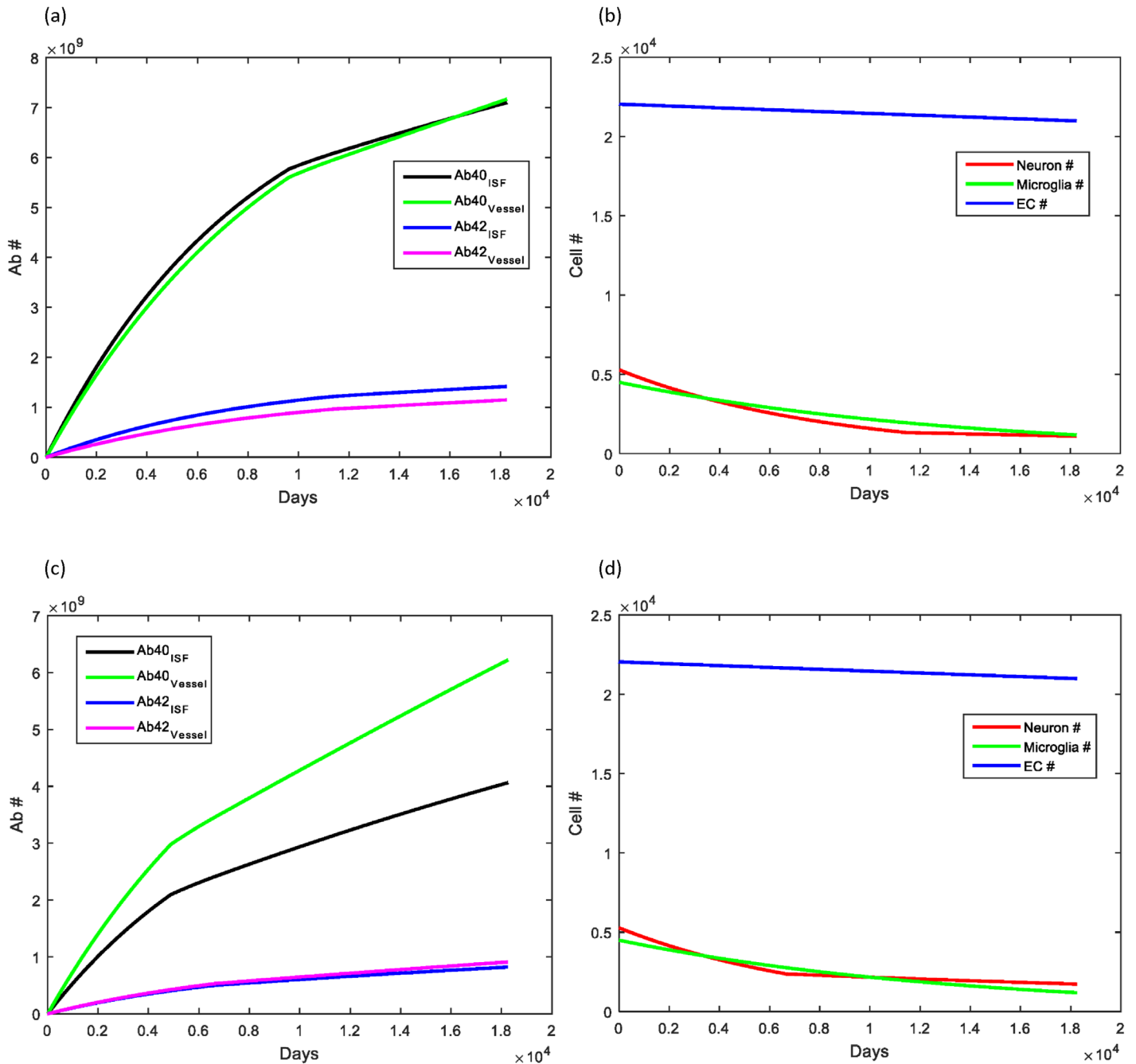


Fig 4. Effect of heart rate on Aβ clearance and deposition. (A, B) Decreasing the heart rate by only 10 beats per minute (60 to 50) led to nearly a 20% increase in the Aβ deposition in the brain parenchyma and a 5% increase in the cerebral vasculature. (C, D) Increasing heart rate by 30 beats per minute (60 to 90) led to the converse, with Aβ deposition levels in brain parenchyma decreasing about 30% and in the cerebral vessels decreasing about 10%.

doi:10.1371/journal.pone.0139574.g004

A sensitivity analysis was performed on the parameters that were estimated instead of derived from the literature (Fig 8). Changes in the initial concentration of beta amyloid within the perivascular space (C_2/C_5) were studied from a range of $\frac{1}{2}$ normal to 2 times normal with no changes in the simulation results observed, suggesting that the model is stable for changes in this value. Analysis on the stability of the k_4 rate constant (the increase in beta amyloid

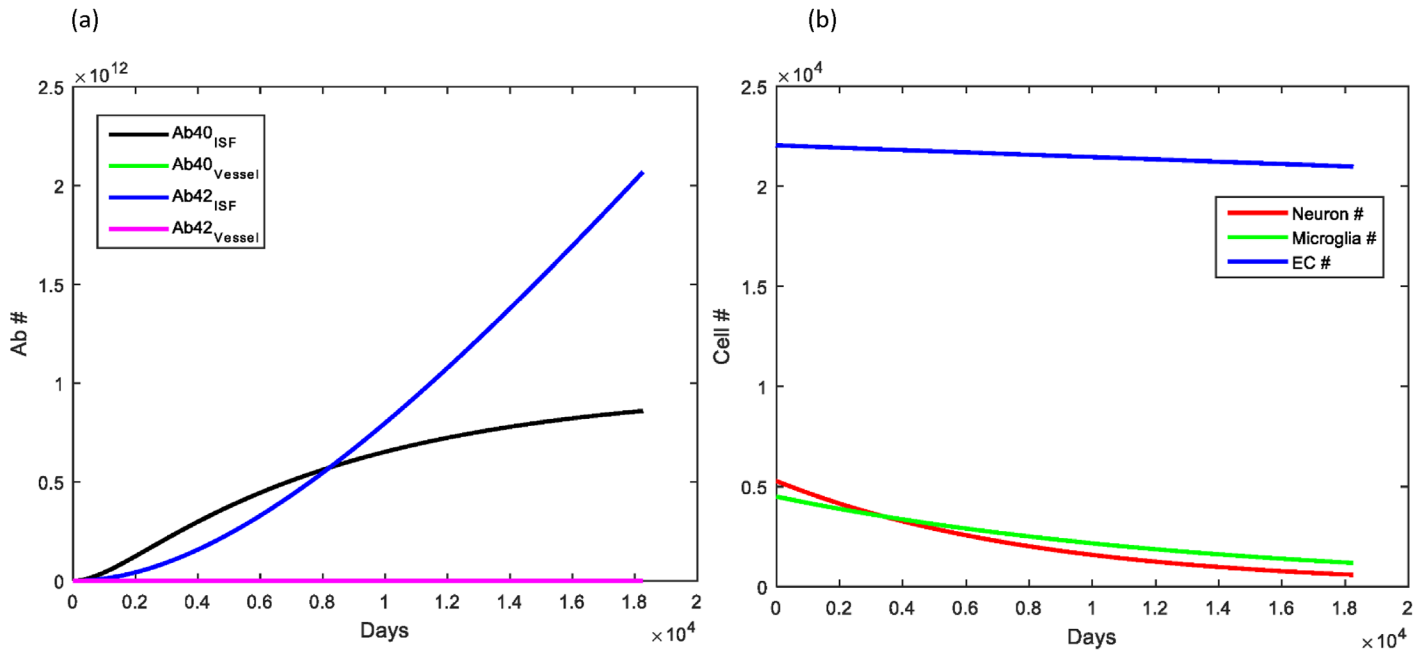


Fig 5. Effect of vessel stiffness on A β clearance and deposition. (A) Increasing the stiffness slowly by a factor of 2 during aging led to a significant increase in the amount of A β deposited within the brain parenchyma, with a decrease in the amount reaching and thus depositing in cerebral vessels. (B) The high A β levels in the brain parenchyma led to accelerated neuronal loss with no change observed in microglia or brain endothelial cell number.

doi:10.1371/journal.pone.0139574.g005

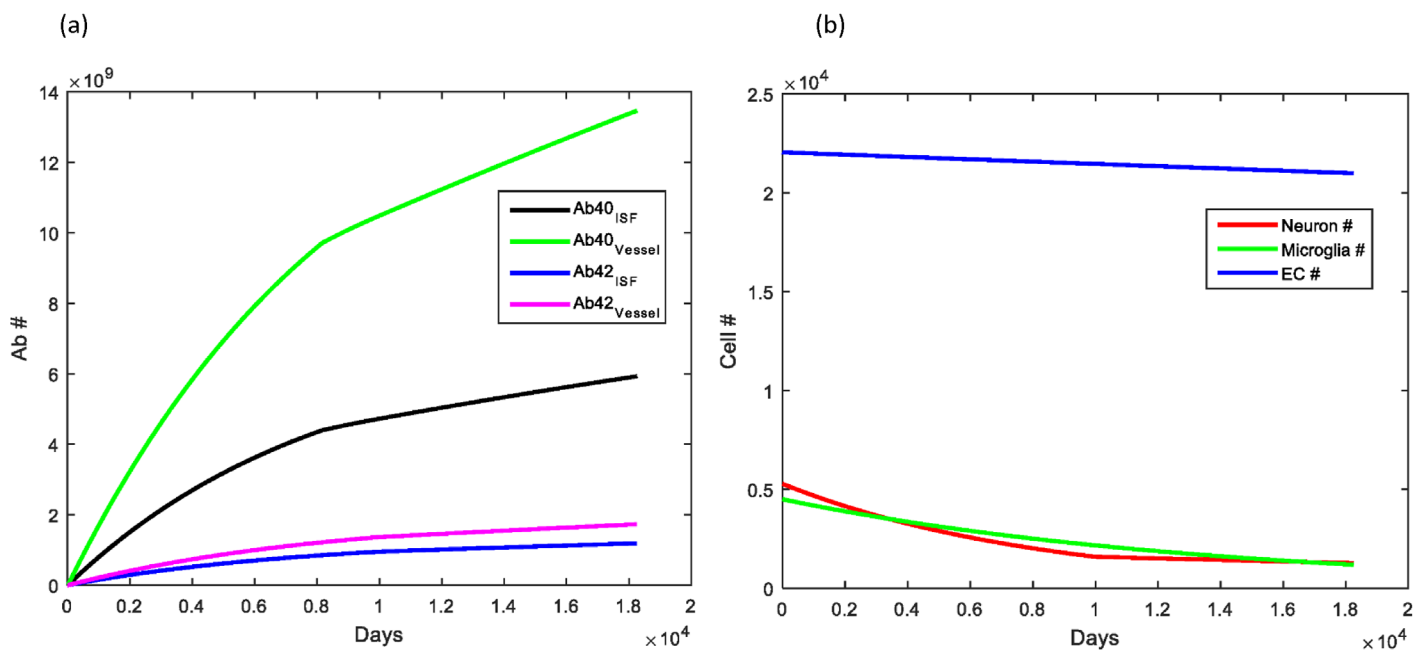


Fig 6. Effect of ApoE allele on A β clearance and deposition. (A) Levels of A β 40 deposition in cerebral vessels increased nearly two-fold with only a 67% increase in A β 42 deposition there. No changes from baseline simulations were noted in A β levels in the brain parenchyma. (B) No changes in cell number were observed compared to baseline values for aging.

doi:10.1371/journal.pone.0139574.g006

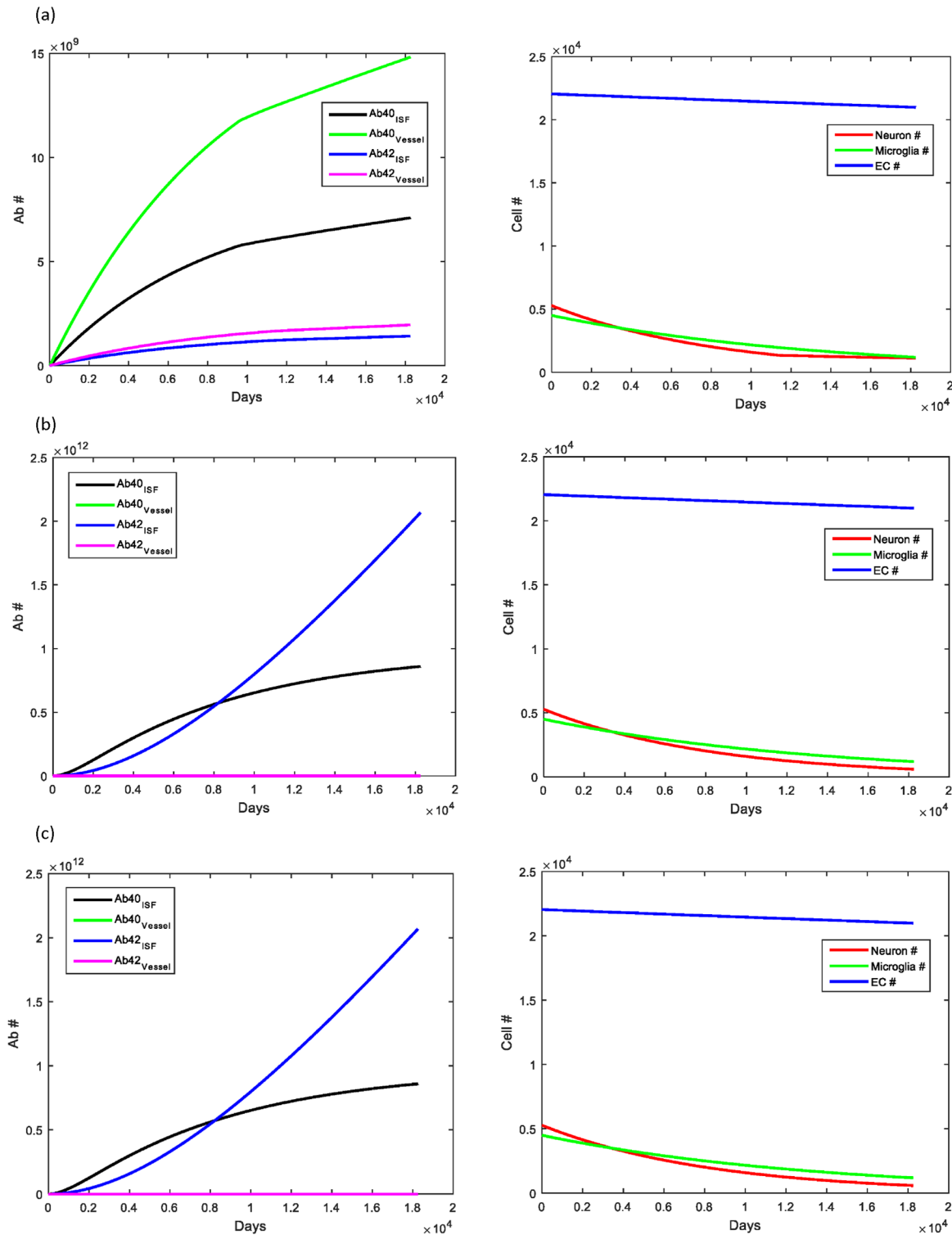


Fig 7. Combination effect of bradycardia, ApoE4 allele and increased vessel stiffness. (A) Having both bradycardia and the ApoE4 allele led to elevated levels of A β 40 deposition in both the brain parenchyma and the cerebral vessels, with nearly a two-fold increase in A β 40 in the cerebral vessels. There was a small decrease in the number of neurons at the final simulation endpoint (<10%). (B) In the case where the simulated patient was supposed to have cardiovascular disease (represented by increased vessel stiffness) and carry the ApoE4 allele, A β deposition was significantly elevated within the brain parenchyma (100x and 1000x for A β 40 and A β 42, respectively). The decreased levels of A β within the cerebrovasculature was not quite as significant as with increased vessel stiffness alone, suggesting that the ApoE allele plays an important role in determining deposition and A β concentration within the space

near cerebral vessels. The significantly elevated Aβ levels led to a decrease in the neuronal cell number secondary to increased neuronal death rate seen at high Aβ levels. (C) The results of increased vessel stiffness in the presence of bradycardia led to results that were similar to those seen with increased vessel stiffness alone.

doi:10.1371/journal.pone.0139574.g007

generation in response to stimuli such as elevated levels of Aβ) demonstrated a narrow range of stability. Increasing k_4 to 2 from 1.5 led to almost a 30% increase in Aβ levels in all compartments modeled. Further increases in k_4 (not shown) continued to show a similar trend.

Discussion

The mathematical model developed in this paper studies the role that clearance by the glymphatic system and LRP-1 at the blood-brain barrier plays in pathogenesis of AD. Altered

Table 3. Summary of simulation results.

Aβ in:	Brain parenchyma	Cerebral Vessel
Normal aging	5.929x10 ⁹	6.8575x10 ⁹
	1.187x10 ⁹	1.0685x10 ⁹
Bradycardia (HR = 50)	1.20	1.05
	1.19	1.07
Elevated HR (HR = 90)	68.5	90.7
	69.2	85.1
Elevated vessel stiffness (2x)	144.92	9.04x10 ⁻⁶
	1741.45	9.07x10 ⁻⁶
ApoE4 allele	No change	1.96
	No change	1.62
ApoE4 allele & bradycardia (HR = 50)	1.20	2.16
	1.19	1.83
ApoE4 allele & increased vessel stiffness	144.92	2.9x10 ⁻⁵
	1741.45	2.98x10 ⁻⁴
Bradycardia & increased vessel stiffness	144.92	9.04x10 ⁻⁶
	1741.45	9.07x10 ⁻⁶
Increased beta amyloid generation (2x)	1.31	1.29
	1.30	1.30

Under normal aging, Aβ₄₀ within the brain parenchyma was found to be 5.929x10⁹, while Aβ₄₂ in the brain parenchyma was 1.187x10⁹. Within the cerebral vessel, Aβ₄₀ was 6.8575x10⁹ and Aβ₄₂ was 1.068x10⁹. The final endpoint value for each simulation was determined and then normalized to the corresponding value obtained for the normal aging simulation to determine the normalized ratio. The normalized ratios for Aβ₄₀ are listed first in each row, followed by the value for Aβ₄₂. The results here show the dramatic increase in beta amyloid within the brain parenchyma when vessel stiffness increases slowly during aging to a maximum two-fold increase. There is also a corresponding decrease in the amount of Aβ at the cerebral vessel. The only simulation condition that showed a decrease in Aβ was the elevated heart rate to 90 beats per minute. This simulation was trying to model the effect of daily exercise on Aβ clearance and demonstrated the efficacy of exercise in helping to increase Aβ clearance. The final row describes the Aβ normalized ratio when Aβ generation is increased two-fold as part of the sensitivity analysis. This simulation demonstrated that increasing Aβ generation rate had an effect similar to bradycardia in the overall levels of Aβ within the brain parenchyma, but led to further elevations in Aβ within the cerebral vasculature with respect to the bradycardia and normal aging simulations. These results suggests that increased Aβ generation alone is not responsible for the elevated levels of Aβ seen in the brains of patients with AD, though the role of vessel stiffness may play a very important role.

doi:10.1371/journal.pone.0139574.t003

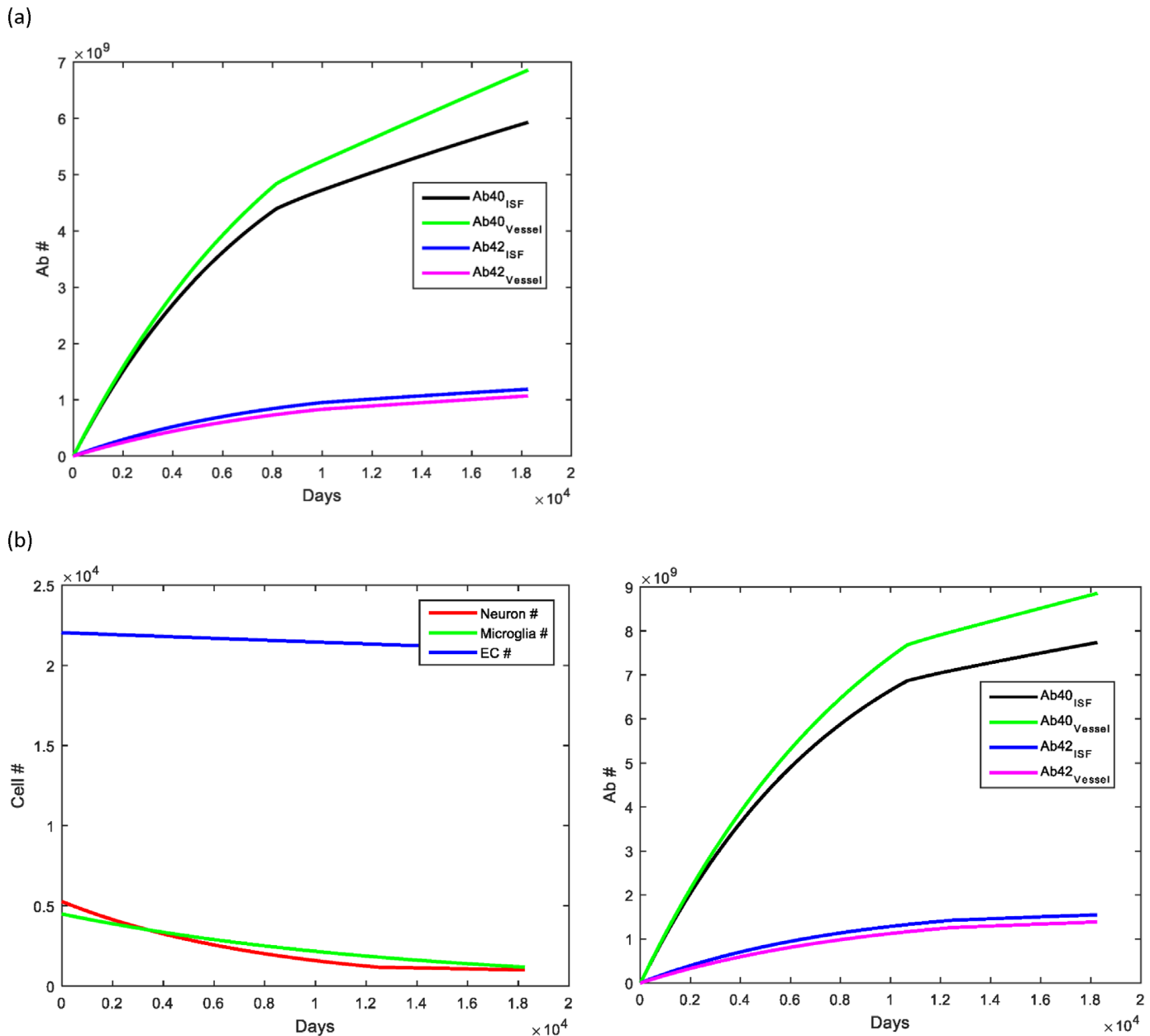


Fig 8. Sensitivity analysis of the model. (A) The sensitivity of the model to values that were estimated was studied to determine the range over which the model produced stable simulation results. Changing the initial concentration of $A\beta$ from $\frac{1}{2}x$ to $2x$ led to no changes in simulation result and demonstrating stability of this rate constant. (B) Changing the amount that $A\beta$ generation would increase in response to a stimulus (k_4) showed that this parameter had a relatively narrow range of stability.

doi:10.1371/journal.pone.0139574.g008

clearance levels have been implicated as causal factors in the development of AD [60–64]. Results of the model for normal aging demonstrated a gradual increase in $A\beta$ deposition in both the brain parenchyma and the cerebral vessels which correlates well to experimental results [5, 35, 49]. Monitoring neuron, microglia and brain endothelial cell numbers allowed us to track the steady decline in functional cells of each type that occurs normally with aging. One of the limitations of this model is that transport of $A\beta$ by diffusion down its concentration gradient from neurons to the BBB was not incorporated as little experimental data is available at

this time. Given what is known of transport properties in the brain, diffusion has been theorized to be an important contributor to movement of chemical species in the brain ISF when species are traveling short distances in the grey matter (few-tens of microns), however, it is believed that convective flow dominates in white matter tracts [26, 65]. Future experimental work will help to better elucidate this mechanism and allow for more accurate modeling.

Cardiovascular risk factors such as the ApoE4 allele, prolonged hypertension leading to re-modeling of vessels and hyperlipidemia have also been recognized as risk factors for AD. In this model, we found that increasing the vessel stiffness by a factor of just 2 from baseline led to a significant increase in the deposition of A β in the brain parenchyma most likely secondary to decreased transfer of arterial pulsations and thus, decreased bulk ISF flow. These simulations clearly demonstrated the importance that changes in vessel structure can have in the clearance of A β from the brain and offer insight into the disease process, as well as a possible modifiable risk factor. Further research looking at the effect of better blood pressure management and prevention of vessel re-modeling and its effect on AD pathogenesis would provide the necessary evidence to determine if this is a viable AD prevention strategy.

Increasing vessel stiffness in combination with having the ApoE4 allele led to a 10-fold increase in A β within the cerebral vasculature compared to the value for increased stiffness only. A similar trend for increased cerebrovasculature deposition of A β was seen in other simulations where the ApoE4 allele was included, suggesting the importance that ApoE4 plays in deposition of A β in the vasculature. Although ApoE4 is not a modifiable risk factor for AD, this model suggests that being a carrier for it may increase ones risk of having cerebrovasculature deposits of A β otherwise known as cerebral amyloid angiopathy (CAA). Further study is still needed to better understand the role that ApoE may play in competitive inhibition of A β transport at the blood-brain barrier and its possible role in CAA.

Studying the effect of elevated heart rate on A β clearance demonstrated that raising heart rate (90 beats per minute) as can happen during exercise, is beneficial for removing A β from the brain. Though this effect was modest, it still demonstrated the positive benefit that exercise can have, especially for the elderly [66–68].

This model represents an attempt to study multi-level interactions between cells within the brain, A β levels, LRP-1 levels and the ApoE allele. Future models should look at the interaction between this system and the role that inflammation and cholesterol processing may play in AD pathogenesis. Sleep is also known to be a major determinant of beta amyloid clearance via the glymphatic system, however, experimental rate constants in humans on how shortened lengths of sleep may affect clearance requires further investigation but would be an important parameter to include in future models [69]. Also, as further *in vivo* research that accurately measures parameters for diffusion and convection in the brain become available, including the role of the aquaporin-4 receptor in the glymphatic clearance pathway, the model can be refined to include these newer parameters to more accurately model the system and increase our understanding of divergence of AD progression from normal aging [11, 70].

Acknowledgments

CRK would like to thank the library services at the Pennsylvania State University College of Medicine for their help and resources while preparing this manuscript.

Author Contributions

Conceived and designed the experiments: CRK JSB. Performed the experiments: CRK JSB. Analyzed the data: CRK JSB. Contributed reagents/materials/analysis tools: CRK JSB. Wrote the paper: CRK JSB. Wrote Matlab code: CRK.

References

1. Querfurth HW, LaFerla FM. Alzheimer's Disease, *N Engl J Med* 2010; 362 (4): 329–44. doi: [10.1056/NEJMra0909142](https://doi.org/10.1056/NEJMra0909142) PMID: [20107219](https://pubmed.ncbi.nlm.nih.gov/20107219/)
2. Karran E, Mercken M, De Strooper B. The amyloid cascade hypothesis for Alzheimer's disease: an appraisal for the development of therapeutics. *Nature reviews*. 2011 Sept; 10(9):698–712. doi: [10.1038/nrd3505](https://doi.org/10.1038/nrd3505) PMID: [21852788](https://pubmed.ncbi.nlm.nih.gov/21852788/)
3. Kanekiyo T, Xu H, Bu G. ApoE and Abeta in Alzheimer's disease: accidental encounters or partners? *Neuron*. 2013 Feb 19; 81(4):740–754.
4. Cirrito JR, May PC, O'Dell MA, Taylor JW, Parsadanian M, Cramer JW, et al. In vivo assessment of brain interstitial fluid with microdialysis reveals plaque-associated changes in amyloid-beta metabolism and half-life. *J Neurosci*. 2003 Oct 1; 23(26):8844–8853. PMID: [14523085](https://pubmed.ncbi.nlm.nih.gov/14523085/)
5. Marklund N, Blennow K, Zetterberg H, Ronne-Engstrom E, Enblad P, Hillered L. Monitoring of brain interstitial total tau and beta amyloid proteins by microdialysis in patients with traumatic brain injury. *Journal of neurosurgery*. 2009 Jun; 110(6):1227–1237. doi: [10.3171/2008.9.JNS08584](https://doi.org/10.3171/2008.9.JNS08584) PMID: [19216653](https://pubmed.ncbi.nlm.nih.gov/19216653/)
6. Mura E, Lanni C, Preda S, Pistoia F, Sara M, Racchi M, et al. Beta-amyloid: a disease target or a synaptic regulator affecting age-related neurotransmitter changes? *Current pharmaceutical design*. 2010; 16 (6):672–683. PMID: [20388077](https://pubmed.ncbi.nlm.nih.gov/20388077/)
7. Rodrigue KM, Kennedy KM, Park DC. Beta-amyloid deposition and the aging brain, *Neuropsychol Rev*, 2009; 19: 436–450. doi: [10.1007/s11065-009-9118-x](https://doi.org/10.1007/s11065-009-9118-x) PMID: [19908146](https://pubmed.ncbi.nlm.nih.gov/19908146/)
8. Watt AD, Perez KA, Rembach A, Sherrat NA, Hung LW, Johanssen T, et al. Oligomers, fact or artefact? SDS-PAGE induces dimerization of beta-amyloid in human brain samples, *Acta Neuropathol*, 2013; 125:549–564. doi: [10.1007/s00401-013-1083-z](https://doi.org/10.1007/s00401-013-1083-z) PMID: [23354835](https://pubmed.ncbi.nlm.nih.gov/23354835/)
9. Haass C, Selkoe DJ. Soluble protein oligomers in neurodegeneration: lessons from the Alzheimer's amyloid beta-peptide. *Nat Rev Mol Cell Biol*. 2007 Feb; 8(2):101–112. PMID: [17245412](https://pubmed.ncbi.nlm.nih.gov/17245412/)
10. Wyss-Coray T, Rogers J. Inflammation in Alzheimer Disease- A Brief Review of the Basic Science and Clinical Literature, *Cold Spring Harb Perspect Med*, 2012; 2: doi: [10.1101/cshperspect.a006346](https://doi.org/10.1101/cshperspect.a006346)
11. Iliff JJ, Wang M, Liao Y, Plogg BA, Peng W, Gundersen GA, et al. A paravascular pathway facilitates CSF flow through the brain parenchyma and the clearance of interstitial solutes, including amyloid beta, *Sci Transl Med* 2012; 4(147): doi: [10.1126/scitranslmed.3003748](https://doi.org/10.1126/scitranslmed.3003748)
12. Weller RO, Preston SD, Subash M, Carare RO. Cerebral amyloid angiopathy in the aetiology and immunotherapy of Alzheimer disease, *Alzheimers Res Ther*, 1 2009; 1(2): doi: [10.1186/alzrt6](https://doi.org/10.1186/alzrt6)
13. Iliff JJ, Wang M, Zeppenfeld DM, Venkataraman A, Plog BA, Liao et al., Cerebral arterial pulsation drives paravascular CSF-interstitial fluid exchange in the murine brain, *J Neurosci* 2013; 33 (46):18190–18199. doi: [10.1523/JNEUROSCI.1592-13.2013](https://doi.org/10.1523/JNEUROSCI.1592-13.2013) PMID: [24227727](https://pubmed.ncbi.nlm.nih.gov/24227727/)
14. Hawkes CA, Sullivan PM, Hands S, Weller RO, Nicoll JAR, Carare RO, Disruption of Arterial Perivascular Drainage of Amyloid- β from the Brains of Mice Expressing the Human APOE ϵ 4 Allele. *PLoS ONE* 2012; 7: e41636. doi: [10.1371/journal.pone.0041636](https://doi.org/10.1371/journal.pone.0041636) PMID: [22848551](https://pubmed.ncbi.nlm.nih.gov/22848551/)
15. Grimmer T, Goldhardt O, Guo LH, Yousefi BH, Forster S, Drzezga A, et al. LRP-1 polymorphism is associated with global and regional amyloid load in Alzheimer's disease in humans in-vivo, *Neuroimage Clin*, 2014; 4: 411–416. doi: [10.1016/j.nicl.2014.01.016](https://doi.org/10.1016/j.nicl.2014.01.016) PMID: [24596678](https://pubmed.ncbi.nlm.nih.gov/24596678/)
16. Morris AW, Carare RO, Schreiber S, Hawkes CA. The Cerebrovascular Basement Membrane: Role in the Clearance of beta-amyloid and Cerebral Amyloid Angiopathy, *Front Aging Neurosci*, 2014; 6: 251. doi: [10.3389/fnagi.2014.00251](https://doi.org/10.3389/fnagi.2014.00251) PMID: [25285078](https://pubmed.ncbi.nlm.nih.gov/25285078/)
17. Cirrito JR, May PC, O'Dell MA, Taylor JW, Parsadanian M, Cramer JW, et al. In vivo assessment of brain interstitial fluid with microdialysis reveals plaque-associated changes in amyloid-beta metabolism and half-life, *J Neurosci* 2003; 23:8844–8853. PMID: [14523085](https://pubmed.ncbi.nlm.nih.gov/14523085/)
18. Gomis M, Sobrino T, Ois A, Millan M, Rodriguez-Campello A, Perez de la Ossa N, et al. Plasma beta-amyloid 1–40 is associated with the diffuse small vessel disease subtype, *Stroke* 2009; 40: 3197–3201. doi: [10.1161/STROKEAHA.109.559641](https://doi.org/10.1161/STROKEAHA.109.559641) PMID: [19696416](https://pubmed.ncbi.nlm.nih.gov/19696416/)
19. Shibata M, Yamada S, Kumar SR, Calero M, Bading J, Frangione B, et al. Clearance of Alzheimer's amyloid-ss(1–40) peptide from brain by LDL receptor-related protein-1 at the blood-brain barrier, *J Clin Invest* 2000; 106: 1489–1499. PMID: [11120756](https://pubmed.ncbi.nlm.nih.gov/11120756/)
20. Lomakin A, Chung DS, Benedek GB, Kirschner DA, Teplow DB. On the nucleation and growth of amyloid beta-protein fibrils: detection of nuclei and quantitation of rate constants, *Proc Natl Acad Sci* 1996; 23: 1125–1129.
21. Pallito MM, Murphy RM. A mathematical model of the kinetics of beta-amyloid fibril growth from the denatured state, *Biophys J* 2001; 81: 1805–1822. PMID: [11509390](https://pubmed.ncbi.nlm.nih.gov/11509390/)

22. Puri IK, Li L. Mathematical Modeling for the Pathogenesis of Alzheimer's Disease, *PLoS ONE* 2010; 5: e. 15176.
23. Luca M, Chavez-Ross A, Edelstein-Keshet L, Mogilner A. Chemotactic signaling, microglia, and Alzheimer's disease senile plaques: is there a connection?, *Bull Math Biol* 2003; 65: 693–730. PMID: [12875339](#)
24. Schuff N, Woerner N, Boreta L, Kornfield T, Shaw LM, Trojanowski JQ, et al. MRI of hippocampal volume loss in early Alzheimer's disease in relation to ApoE genotype and biomarkers, *Brain* 2009; 132: 1067–77. doi: [10.1093/brain/awp007](#) PMID: [19251758](#)
25. Wong AD, Ye M, Levy AF, Rothstein JD, Bergles DE, Searson PC. The blood-brain barrier: an engineering perspective, *Front Neuroeng* 2013; 6: doi: [10.3389/fneng.2013.00007](#)
26. Abbott N. Evidence for bulk flow of brain interstitial fluid: significance for physiology and pathology, *Neurochem Int* 2004; 40: 545–552.
27. Kusumoto Y, Lomakin A, Teplow DB, Benedek GB. Temperature dependence of amyloid beta-protein fibrillization, *Proc Natl Acad Sci* 1998; 95: 12277–12282. PMID: [9770477](#)
28. Filippov AV, Grobner G, Antzutkin ON. Aggregation of amyloid Abeta (1–40) peptide in perdeuterated 2,2,2-trifluoroethanol caused by ultrasound sonication, *Magn Reson Chem* 2010; 48:427–434. doi: [10.1002/mrc.2596](#) PMID: [20474020](#)
29. Dorr A, Sahota B, Chinta LV, Brown ME, Lai AY, Ma K, et al. Amyloid-beta-dependent compromise of microvascular structure and function in a model of Alzheimer's disease, *Brain* 2012; 135: 3039–3050. doi: [10.1093/brain/aws243](#) PMID: [23065792](#)
30. Flanagan TRJ, Emerich DF, Winn SR. Providing pharmacological access to the brain: alternate approaches. San Diego, Ca.: Academic Press 1994.
31. Ottesen JT, Olufsen MS, Larsen JK. Applied Mathematical Models in Human Physiology, SIAM 2004: 18–24.
32. Simic G, Kostovic I, Winblad B, Bogdanovic N. Volume and number of neurons of the human hippocampal formation in normal aging and Alzheimer's disease, *J Comp Neurol* 1997; 379: 482–494. PMID: [9067838](#)
33. Harding AJ, Halliday GM, Kril JJ. Variation in hippocampal neuron number with age and brain volume, *Cereb Cortex* 1998; 8: 710–718. PMID: [9863698](#)
34. Zarow C, Vinters HV, Ellis WG, Weiner MW, Mungas D, White L, et al. Correlates of hippocampal neuron number in Alzheimer's disease and ischemic vascular dementia, *Ann Neurol* 2005; 57: 896–903. PMID: [15929035](#)
35. Fritschi SK, Langer F, Kaeser SA, Maia LF, Portelius E, Pinotsi D, et al. Highly potent soluble amyloid-beta seeds in human Alzheimer brain but not cerebrospinal fluid, *Brain* 2014; 137: 2909–2915. doi: [10.1093/brain/awu255](#) PMID: [25212850](#)
36. Dorr A, Sahota B, Chinta LV, Brown ME, Lai AY, Ma K, et al. Amyloid-beta-dependent compromise of microvascular structure and function in a model of Alzheimer's disease. *Brain*. 2012; 135:3039–3050. doi: [10.1093/brain/aws243](#) PMID: [23065792](#)
37. Mura E, Lanni C, Preda S, Pistoia F, Sara M, Racchi M, et al. Beta-amyloid: a disease target or a synaptic regulator affecting age-related neurotransmitter changes? *Current pharmaceutical design* 2010; 16:672–683. PMID: [20388077](#)
38. Tetreault NA, Hakeem AY, Jiang S, Williams BA, Allman E, Wold BJ, et al. Microglia in the cerebral cortex in autism, *J Autism Dev Disord* 2012; 42(12): 2569–2584. doi: [10.1007/s10803-012-1513-0](#) PMID: [22466688](#)
39. Pelvig DP, Pakkenberg H, Stark AK, Pakkenberg B. Neocortical glial cell numbers in human brains, *Neurobiol Aging* 2008; 29: 1754–1762. PMID: [17544173](#)
40. Streit WJ, Sammons NW, Kuhns AJ, Sparks DL. Dystrophic microglia in the aging human brain, *Glia* 2004; 45: 208–212. PMID: [14730714](#)
41. Pardridge WM. Blood-brain barrier biology and methodology. *Journal of neurovirology* 1999 Dec; 5(6):556–569. PMID: [10602397](#)
42. Garipcan B, Maenz S, Pham T, Settmacher U, Jandt KD, Zanow J, et al. Image Analysis of Endothelial Microstructure and Endothelial Cell Dimensions of Human Arteries- A Preliminary Study, *Advanced Engineering Materials* 2011; 13: B54–B57.
43. Helliwell T, Smith P, Heath D. Endothelial pavement patterns in human arteries, *J Pathol* 1982; 136: 227–240. PMID: [6175739](#)
44. Ye M, Sanchez HM, Hultz M, Yang Z, Bogorad M, Wong AD, et al. Brain microvascular endothelial cells resist elongation due to curvature and shear stress, *Sci Rep* 2014 Apr 15; 4: doi: [10.1038/srep04681](#)

45. Cines DB, Pollak ES, Buck CA, Loscalzo J, Zimmerman GA, McEver RP, et al. Endothelial Cells in Physiology and in the Pathophysiology of Vascular Disorders, *Blood* 1998; 91: 3527–3561. PMID: [9572988](#)
46. Sane D. The endothelial life insurance plan, *Blood* 2004; 104: 2615–2616.
47. Op den Buijs J, Musters M, Verrips T, Post JA, Braam B, van Riel N, Mathematical modeling of vascular endothelial layer maintenance: the role of endothelial cell division, progenitor cell homing, and telomere shortening, *Am J Physiol Heart Circ Physiol* 2004; 287: H2651–8. PMID: [15284068](#)
48. Krouwer VJ, Hekking LH, Langelaar-Makkinje M, Regan-Klapisz E, Post JA. Endothelial cell senescence is associated with disrupted cell-cell junctions and increased monolayer permeability, *Vasc Cell* 2012; 4: doi: [10.1186/2045-824X-4-12](#)
49. Dang S, Wu S, Wang J, Li H, Huang M, He W, et al. Cleavage of amyloid precursor protein by an archaeal presenilin homologue PSH, *Proc Natl Acad Sci U S A* 2015 Mar 15; 112(11): 3344–3349. doi: [10.1073/pnas.1502150112](#) PMID: [25733893](#)
50. Deane R, Sagare A, Zlokovic BV. The role of the cell surface LRP and soluble LRP in blood-brain barrier Abeta clearance in Alzheimer's disease, *Curr Pharm Des* 2008; 14: 1601–1605. PMID: [18673201](#)
51. Verghese PB, Castellano JM, Garai K, Wang Y, Jiang H, Shah A, et al. ApoE influences amyloid-beta (Abeta) clearance despite minimal apoE/Abeta association in physiological conditions, *Proc Natl Acad Sci U S A* 2013 May 7; 110(19): E1807–16. doi: [10.1073/pnas.1220484110](#) PMID: [23620513](#)
52. Wildsmith KR, Holley M, Savage JC, Skerrett R, Landreth GE. Evidence for impaired amyloid beta clearance in Alzheimer's disease, *Alzheimers Res Ther* 2013 July 12; 5: doi: [10.1186/alzrt187](#)
53. Bell RD, Sagare AP, Friedman AE, Bedi GS, Holtzman DM, Deane R, et al. Transport pathways for clearance of human Alzheimer's amyloid beta-peptide and apolipoproteins E and J in the mouse central nervous system, *J Cereb Blood Flow Metab* 2007; 27: 909–918. PMID: [17077814](#)
54. Bachmeier C, Paris D, Beaulieu-Abdelahad D, Mouzon B, Mullan M, Crawford F. A multifaceted role for apoE in the clearance of beta-amyloid across the blood-brain barrier, *Neurodegener Dis* 2013; 11(1): 13–21. PMID: [22572854](#)
55. Ito S, Matsumiya K, Ohtsuki S, Kamiie J, Terasaki T. Contributions of degradation and brain-to-blood elimination across the blood-brain barrier to cerebral clearance of human amyloid-beta peptide(1–40) in mouse brain, *J Cereb Blood Flow Metab* 2013 Nov; 33(11): 1770–1777. doi: [10.1038/jcbfm.2013.125](#) PMID: [23963369](#)
56. Castellano JM, Kim J, Stewart FR, Jiang H, DeMattos RB, Patterson BW, et al, Human apoE isoforms differentially regulate brain amyloid-beta peptide clearance, *Sci Transl Med* 2011 June; 3(89): 89ra57, doi: [10.1126/scitranslmed.3002156](#) PMID: [21715678](#)
57. Lind G, Linsmeier CE, Schouenborg J. The density difference between tissue and neural probes is a key factor for glial scarring, *Sci Rep* 2013; 3, doi: [10.1038/srep02942](#)
58. HvidbergV Maniecki MB, Jacobsen C, Hojrup P, Moller HJ, Moestrup SK. Identification of the receptor scavenging hemopexin-heme complexes, *Blood* 2005; 106: 2572–2579. PMID: [15947085](#)
59. Mahley RW, Weisgraber KH, Huang Y. Apolipoprotein E: structure determines function, from atherosclerosis to Alzheimer's disease to AIDS, *J Lipid Res* 2009; 50: S183–188. doi: [10.1194/jlr.R800069-JLR200](#) PMID: [19106071](#)
60. Vasilevko V, Passos GF, Quiring D, Head E, Kim RC, Fisher M, et al. Aging and cerebrovascular dysfunction: contribution of hypertension, cerebral amyloid angiopathy, and immunotherapy, *Ann N Y Acad Sci* 2010 Oct; 1207: 58–70. doi: [10.1111/j.1749-6632.2010.05786.x](#) PMID: [20955427](#)
61. Yoon SS, Jo SA. Mechanisms of Amyloid-beta Peptide Clearance: Potential Therapeutic Targets for Alzheimer's Disease, *Biomol Ther (Seoul)* 2012 May; 20(3): 245–255.
62. Castellano JM, Deane R, Gottesdiener AJ, Verghese PB, Stewart FR, West T, et al. Low-density lipoprotein receptor overexpression enhances the rate of brain-to-blood Abeta clearance in a mouse model of beta-amyloidosis, *Proc Natl Acad Sci U S A* 2012 Sept; 109(38): 15502–15507. PMID: [22927427](#)
63. Elahy M, Jackaman C, Mamo JC, Lam V, Dhaliwal SS, Giles C, Nelson D, Takechi R. Blood-brain barrier dysfunction developed during normal aging is associated with inflammation and loss of tight junctions but not with leukocyte recruitment, *Immun Ageing* 2015; 12: 2, doi: [10.1186/s12979-015-0029-9](#) PMID: [25784952](#)
64. Kress BT, Iliff JJ, Xia M, Wang M, Wei HS, Zeppenfeld D, et al. Impairment of paravascular clearance pathways in the aging brain. *Annals of neurology* 2014 Dec; 76(6): 845–861. doi: [10.1002/ana.24271](#) PMID: [25204284](#)
65. Brinker T, Stopa E, Morrison J, Klinge P. A new look at cerebrospinal fluid circulation, *Fluids Barriers CNS* 2014 May; 11: 10, doi: [10.1186/2045-8118-11-10](#) PMID: [24817998](#)

66. Lange-Asschenfeldt C, Kojda G. Alzheimer's disease, cerebrovascular dysfunction and the benefits of exercise: From vessels to neurons, *Exp Gerontol* 2008; 43: 499–504. doi: [10.1016/j.exger.2008.04.002](https://doi.org/10.1016/j.exger.2008.04.002) PMID: [18474414](https://pubmed.ncbi.nlm.nih.gov/18474414/)
67. Adlard PA, Perreau VM, Pop V, Cotman CW. Voluntary Exercise Decreases Amyloid Load in a Transgenic Mouse Model of Alzheimer's Disease, *J Neurosci* 2005; 25: 4217–4221. PMID: [15858047](https://pubmed.ncbi.nlm.nih.gov/15858047/)
68. Cotman CW, Berchtold NC. Exercise: a behavioral intervention to enhance brain health and plasticity, *Trends Neurosci* 2002; 25: 295–301. PMID: [12086747](https://pubmed.ncbi.nlm.nih.gov/12086747/)
69. Xie L, Kang H, Xu Q, Chen MJ, Liao Y, Thiyagarajan M et al. Sleep Drives Metabolite Clearance from the Adult Brain, *Science* 2013; 342: 373–377. doi: [10.1126/science.1241224](https://doi.org/10.1126/science.1241224) PMID: [24136970](https://pubmed.ncbi.nlm.nih.gov/24136970/)
70. Nedergaard M. Garbage Truck of the Brain, *Science* 2013; 340: 1529–1530. doi: [10.1126/science.1240514](https://doi.org/10.1126/science.1240514) PMID: [23812703](https://pubmed.ncbi.nlm.nih.gov/23812703/)